Noctisense: A Contactless Sleep Monitoring System

Mason Miles[1], Jose Ojeda[1], Colby Toner[1], and Edward Perez[1]

[1]Department of Electrical Engineering and Computer Science, University of Central Florida, Orlando, Florida 32816 USA

ABSTRACT

Noctisense is a contactless sleep monitoring system designed to track sleep patterns and generate sleep quality scores without the need for wearable devices. It utilizes a combination of thermal imaging and radar technology to monitor the user from a bedside position. The system is integrated into a lamp design, allowing it to function as a standard light source while unobtrusively capturing biometric data. By utilizing various sensors, Noctisense monitors body temperature, movement, and acoustic disturbances to build a comprehensive sleep profile without the recurring costs or privacy concerns associated with cloud-dependent commercial alternatives.

Keywords: Contactless monitoring, Doppler radar, infrared sensors, sleep tracking, thermal imaging, embedded systems, mobile health.

1. INTRODUCTION

Since the early 1970s with the use of actigraphy devices, both health professionals and watchful people have sought to gain insight into their health through the monitoring of sleep.[1] While the market for such devices was initially restricted to medical practices and researchers, the early 2000s to the mid-2010s brought forth a boom of all consumer wearable devices thanks to the coinciding rise of the semiconductor industry. Alongside the rise of wearable devices, the demand for individual health data tracking continues to grow year over year. Industry analysts estimate the global sleep-tracking device market at roughly $26.6 billion in 2023, projected to reach $58.2 billion by 2030,[2] underscoring both the scale of consumer interest and the intensity of competition Noctisense enters.

The most common variant of consumer devices used to measure this data is by far the smart watch, with some market share in recent years shifting towards a new smart ring category of devices. Amongst these devices, there is a common barrier to continued use in both having to wear a physical sensor whilst sleeping, along with maintaining the device.

One recent product by the name of Eight Sleep aimed to avoid this pitfall by implementing their sensors via a mattress cover, which based on consumer feedback, affirms the belief that the most ideal solution to sleep tracking is a non-wearable methodology.[3] However, even with Eight Sleep solving the first barrier to lasting consumer adoption, it shares an arguably even greater blocking factor with many of its predecessors: a subscription model.

Table 1 summarizes list pricing and subscription terms compiled by the design team for four representative commercial offerings against the intended cost structure of Noctisense. Every incumbent surveyed, whether wrist-, finger-, or mattress-based, carries a recurring annual fee on top of the hardware purchase, and all disclose that user data is used to train the manufacturer's proprietary algorithms.

Noctisense aims to eliminate all of the previously stated barriers through non-intrusive sleep data measurement, locally-stored data with no cloud or subscription services, and no erroneous features.

2. GOALS AND OBJECTIVES

The design of Noctisense is guided by four overarching pillars established at the outset of the project: (1) measuring data that is actually meaningful to sleep hygiene, body and room temperature, restless movement, heart and respiratory rate, and audio disturbances, rather than vanity metrics. (2) Digesting and displaying that data through a friendly, actionable mobile interface; (3) cross-validating measurements across multiple independent sensors so that reported values remain realistic rather than alarming; and (4) ensuring the hardware itself is safe through deliberate power distribution, thermal, and data-privacy design. These pillars are decomposed into the base, advanced goals, and core objectives below, followed by the engineering requirements used to make each objective measurable.

Table 1. Commercial Sleep-Tracking Device Comparison

Device	Price	Subscription	Data Use
Smart watch*	\$249–\$1,399	Requires host phone	Trains vendor AI
Smart band	\$399–\$499	\$70/yr	Trains vendor AI
Smart ring	N/A†	\$199–\$359/yr	Trains vendor AI
Mattress cover	\$2,849–\$5,899	\$199–\$399/yr	Trains vendor AI
Noctisense	**≤\$200 (est.)**	**\$0**	**None**

2.1 Base Goals

- Utilize thermal imaging sensor to record body temperature throughout the night.
- Implement restless movement tracking via 24 GHz mmWave radar tracking.
- Record audible disruptions during sleep period.
- Person detection using NIR optical subsystem.

2.2 Advanced Goals

- Develop a user-friendly mobile application for displaying sleep data and audio clips, along with system configuration controls such as bedtime system automation.
- Measure respiratory/heart rate using 24 GHz mmWave radar tracking.
- Design and build an aesthetically pleasing housing for the sensors that is consumer-friendly.
- Compare NIR optical system with commercial products and have lower cost with high quality.

2.3 Core Objectives

- **Average Body Temperature:** Using a thermal image capture every sampling period, normalize pixel values that represent the heat map to account for environmental conditions. Then apply noise filtering using Gaussian blurring and detect hotspots by identifying pixels above a certain threshold and track their changes over time.
- **Restless Movement:** Using a 24GHz mmWave radar signal, specifically the MR24BSD1 radar module by Seeed Studios. Record instances of movement over a defined threshold tuned to the individual user through integrated DSP libraries within the module. Then, report total instance count of restless movement to the user via application.
- **Sound Tracking:** Monitor audio data with the signal normalized to environmental conditions. When a triggering event over the set dB threshold occurs, feed data into an LAME MP3 encoder to be stored until the end of a defined event period (5s). Then, store this clip in its compressed format on the SD-flash storage.
- **In-Bed Detection:** Determine whether a person is physically present on the bed by detecting reflected infrared light from the user's upper torso using a continuous beam subsystem.

2.4 Engineering Requirements

Each objective above was translated into a quantifiable engineering requirement so that progress could be demoed and verified rather than asserted. Table 2 lists the six parameters carried forward from Senior Design I into the demonstrable criteria used at both the midterm demo and the critical design review.

Table 2. **System Engineering Requirements and Target Values**

Parameter	**Description**	**Target Value**
Monitoring Area	Maximum area the device can effectively track, based on the combined field of view of the sensor suite; wide enough that the user is not constrained in lamp placement, but narrow enough that the sensors can reliably localize the user.	2850 in^2
Lamp Housing Footprint	Overall dimensions of the lamp housing.	19.7 in W × 23.6 in H
Operation / Setup	Total time for a data update to process on-device, transmit, and populate in the mobile application, measured from the time of connection.	Synchronized within <1 m
Operating Voltage	Nominal device operating voltage.	5 V
Usability	Combined hardware and application setup time, based on execution time plus connection latency.	10 minutes
Optical Detection Distance	Minimum distance over which the optical subsystem must reliably send and receive its signal.	≥1.5 m

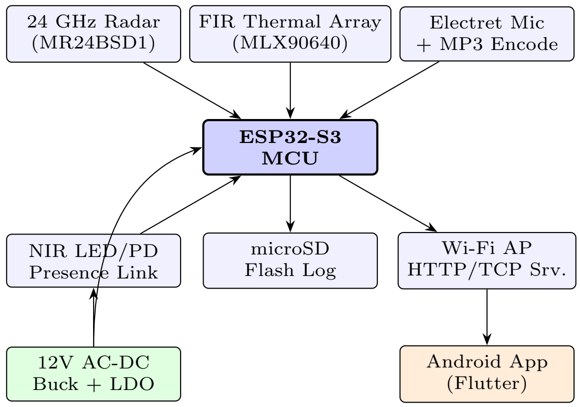

Figure 1. High-level hardware architecture. The four sensing branches feed the ESP32-S3, which logs to microSD and serves telemetry to the Flutter mobile application over the lamp's local Wi-Fi network.

3. HARDWARE DESIGN

The system incorporates several forms of data collection, including thermal imaging, radar, acoustic microphones, and NIR ToF data, all consolidated onto a central microcontroller board that is supported by three peripheral boards: a power/regulator board, an optical board, and a microphone board (Fig. 1). Each subsystem below was selected only after an explicit trade study against at least two alternative technologies, a process the team carried through from the preliminary design phase into the critical design review as more field data became available.

3.1 Main Processor Selection

The system incorporates several forms of data collection, including thermal imaging, radar, acoustic microphones, and NIR Binary Pe data. The ESP32-S3-N16-R8 was selected as it provides ample support for all sensor data as well as capacity for future growth. As summarized in Table 3, the ESP32-S3 was weighed against an ARM Cortex-M4-class option from the Arduino Nano series; the deciding factors were the ESP32-S3's dual-core 240 MHz Xtensa LX7 processor, its native Wi-Fi radio, and the maturity of its community tooling and documentation, all at roughly a third of the competing part's unit cost.[4]

3.2 Movement and Respiratory/Heart Rate Tracking

Millimeter-wave radar works on Doppler principles to detect velocity or displacement. The Seeed MR24BSD1 outputs raw radar frames, decoded by its library into motion states. Integration is straightforward, requiring 5V/GND and connection to the ESP32's serial port. Three sensing modalities were evaluated for this role (Table 4): passive infrared (PIR), RGB-D depth cameras, and mmWave radar. PIR was eliminated first, as its binary presence/absence output offered too little granularity to derive vital-sign data. RGB-D was eliminated

Table 3. **MCU Candidate Comparison**

Attribute	ESP32-S3	ARM Cortex-M4
Clock speed	Dual-core, 240 MHz	Up to 48 MHz
Flash memory	8 MB	256 KB
Wireless	Native Wi-Fi + I/O	I/O only, no Wi-Fi
Unit cost	$5	$13

Table 4. **Movement-Sensing Technology Comparison**

	Radar	PIR	RGB-D
Sampling	Fast	Low	High
Range	Moderate	Far	Far
Vital signs	Yes	No	External proc.
Through wall	Yes	No	No
Cost	$25–$35	$5–$10	$100+

next on cost and its requirement for external processing hardware. Radar was retained for its fast sampling rate, sufficient sensitivity to resolve respiratory and heart-rate signatures, and its ability to operate through the thin plastic wall of the lamp housing.

Having settled on radar as the sensing modality, four 24–60 GHz radar modules were compared directly (Table 5). The Seeed MR24BSD1 was the only candidate developed specifically for sleep tracking, shipping with built-in DSP and a software library exposing breathing, bed-state, and motion functions directly, which made it the most suitable option at its price point despite its comparatively low raw data rate.[5]

3.3 In-Bed Detection (Optical)

A continuous-beam optical subsystem is used to detect a reflective target at distances of up to approximately 1.5 m. The system employs two aspheric condenser lenses to maximize optical coupling between the transmitter, target, and receiver. A 940 nm near-infrared (NIR) LED is positioned at the focal point of the transmitting lens to produce a concentrated beam with reduced divergence, increasing the optical irradiance incident on the target. A second aspheric condenser lens collects the reflected light and focuses it onto a silicon photodiode, significantly increasing the received optical power compared to an unassisted detector. Both theoretical modeling and experimental measurements demonstrated an increase in received optical power from the nanowatt range to the microwatt range, enabling reliable signal acquisition at the required operating distance.

The LED is intensity modulated with a 50% duty cycle, and the reflected signal is synchronously detected by the receiver to reject ambient light interference. Preliminary designs investigated a laser-based time-of-flight ranging architecture; however, the trade studies below conducted ahead of the critical design review favored a lower-complexity, inherently eye-safer architecture once it became clear that only binary presence detection, not absolute ranging, was required for this objective.

3.3.1 Technology Selection

Table 6 compares three depth-sensing principles. The Michelson interferometer was eliminated first: it offers only millimeter-to-centimeter displacement sensing and demands vibration stability below $\lambda/10$ ($\sim$100 nm), which is impractical outside a controlled lab bench. A structured-light camera was eliminated next, since it fails outright in ambient sunlight above 10^4 lux and its triangulation baseline becomes exponentially harder to align as tolerances tighten. A "light tripwire" an intensity-difference measurement rather than a phase- or triangulation-based one was retained, since it reduces the problem to a much simpler binary detection at a fraction of the cost.

3.3.2 Hardware Selection

Within the light-tripwire architecture, an LED emitter was chosen over a laser diode (Table 7). The TSAL6400 IR LED keeps peak optical power around 40 mW, placing it safely in eye-safety Class 1, versus the SPL TL90AT03 laser diode's $\sim$65 W peak power in the more restrictive Class 1–2 band. The LED's 100 mA drive current is also far easier to source reliably than the laser diode's $\sim$3 A, and its 200 mm beam divergence provides a wide

Table 5. **24–60 GHz Radar Module Comparison**

	MR24BSD1	SEN0395	HLK-LD2410	A111
Freq.	24 GHz	24 GHz	24 GHz	60 GHz
Purpose	Sleep track.	Presence	Presence	Multi
DSP	Built-in	Built-in	Community	None
Data rate	Low	Low	Moderate	High
Cost	\$25–\$35	\$20–\$30	\$10–\$20	\$50–\$100

Table 6. **Optical Ranging Technology Comparison**

	Struct. Light	Michelson	Light Tripwire
Principle	Triangulation	Phase diff.	Intensity diff.
Range	0.5–3 m	mm–cm only	0.5–3 m
Constraint	Fails in sun	Sub-$\lambda/10$ stability	Return power
Cost	\$150–\$500	\$1,000+	\$20–\$150

margin against misalignment from an accidental bump, a meaningful concern for hardware that gets repeatedly handled during a multi-semester-long build. At \$0.48 versus \$17+ per unit, the LED is also far more forgiving of the inevitable mistakes made while iterating on a student project.

An aspheric condenser lens (ACL25416U-B, 20.1 mm focal length, NA $\approx$ 0.79) was selected over a longer-focal-length precision-polished alternative. A shorter focal length increases beam divergence and, with it, the risk of losing optical concentration over the 1.5 m link; the chosen lens's numerical aperture comfortably exceeds the LED's own 0.44 NA emission cone (derived from equation 1

$$NA \approx n \sin(\theta) \tag{1}$$

as θ is the LED's divergence of 25° and the refractive index of air n $\approx$ 1). Although the LED is an extended source, accounting for its finite emitting area changes the effective NA only slightly, remaining of the same order of magnitude (.02 difference). Therefore, Eq. 1 provides an adequate approximation for this design. So no emitted light is wasted, at roughly 7.5% of the cost of the precision alternative (\$34.33 vs. \$455).

3.3.3 Link Budget

Radiometry analysis was performed to estimate the optical power transmitted through the sensing path. Without a transmitting condenser lens, approximately 3.3 nW of optical power reaches the target at a distance of 1.5 m. Introducing the aspheric condenser lens reduces beam divergence and increases the incident optical power to approximately 3.3 μW. On the return path, a matching condenser lens significantly increases the fraction of reflected light collected by the photodiode, improving the received optical power from the picowatt range to the microwatt range. A 940 nm narrowband optical filter further improves detection performance by rejecting ambient illumination while transmitting the reflected LED signal. These results justified the dual-lens transmitter/receiver architecture adopted for the final optical subsystem.

3.3.4 Opto-Mechanical Assembly

The LED and photodiode are held at a converging half-angle of 25° toward their respective aspheric lenses in a custom 3D-printed mount. Early prototypes used 3D-printed lens holders as well, but these introduced enough tilt and misalignment during printing that the team moved to a purchased precision lens holder for the final assembly, reserving 3D printing for the LED/photodiode carrier alone.

3.4 Thermal Imaging Module

The MLX90640 Far-Infrared (FIR) thermal sensor array monitors body temperature changes. It uses a 32×24 pixel array to function as a low-resolution thermal camera, tracking the temperature of the sleeper's exposed extremities.[6] As shown in Table 8, an RGB camera was rejected outright for its inability to measure temperature at all and its severe privacy implications in a bedroom setting, while a near-infrared camera was rejected because it resolves only shape and motion, not radiometric temperature, while still exposing identifiable visual features. The FIR array was selected specifically because it captures accurate temperature data while operating in total darkness and preserves privacy, since no facial or identifying features are resolvable in an 8–14 μm thermal image.

Table 7. Optical Emitter Comparison

Metric	TSAL6400 LED	SPL TL90AT03
Peak power	∼0.04 W	∼65 W
Beam divergence	200 mm	9 mm
Drive current	100 mA	∼3 A
Unit cost	$0.48	$17+
Safety class	1	1–2

Table 8. Body-Temperature Sensing Technology Comparison

Technology	Pros	Cons	Selection / Justification
RGB Camera	High resolution, inexpensive.	Requires ambient light; severe privacy concerns; cannot measure temperature.	Violates bedroom privacy requirements and cannot track physiological thermal data.
NIR Camera	Works in total darkness; moderate cost.	Only captures shape/movement, not absolute temperature; identifiable features still visible.	Does not provide radiometric temperature data for sleep-stage analysis.
FIR Thermal	**Accurate temperature data; works in absolute darkness; preserves privacy (no facial features).**	**Lower resolution than optical cameras; computationally heavier.**	**(Selected) ideal for capturing core-adjacent skin temperature safely.**

3.5 Printed Circuit Board Design

Noctisense's electronics are split across four boards, a central MCU/sensor board, a microphone board, an optical board, and a regulator board. Connected by pin-header interfaces rather than direct soldering, so that any single peripheral can be swapped without reworking the rest of the harness. This decision paid off directly during debugging, since a suspect component could be isolated by substitution rather than desoldering. The SD card is the one exception, mounted directly to the main board for mechanical reliability.

The MCU board (2.8 in × 2.8 in, two-layer, 1 oz copper) hosts the ESP32-S3, the radar and thermal-camera headers, the microphone header, the reverse-polarity protection stage, and status/programming headers. The microphone board (0.9 in × 1.5 in) carries the Adafruit MAX4466 reference design plus an added 3.3 V LDO, which proved necessary after the unregulated rail introduced audible artifacting during recording. The optical board (1.9 in × 1.15 in) implements the three-stage emit/receive/rank chain described in Section III-D. The regulator board (1.85 in × 1.1 in, 2 oz copper pour for thermal handling) hosts the cascaded switching-then-linear power stages detailed in Section IV.

All four boards were held to a 1 mm minimum component spacing and standardized on M3 mounting holes to simplify assembly and adhere to JLC's design-for-manufacturing-and-assembly (DFMA) constraints. Hardware protection is provided by a TVS diode for ESD suppression and a P-channel MOSFET reverse-polarity stage whose gate is tied to ground, allowing current to flow only when the external 12 V barrel jack is inserted with correct polarity directly satisfying the hardware-safety objective established in Section II.

4. POWER DELIVERY AND REGULATION

Noctisense uses an external AC-DC conversion stage. To mitigate high-frequency noise from switching regulators, a hybrid regulation approach using low dropout linear regulators after switching buck converters is utilized to provide clean voltage rails. This cascaded topology exists because the system's RF and optical front ends require noise floors that switching regulators alone cannot guarantee: a high-efficiency switching stage first drops the 12 V input to a lower, albeit noisy, intermediate voltage, and a linear regulator then sheds only the small remaining headroom as heat, achieving far higher net efficiency and far less waste heat than a linear-only regulation chain would.

Table 9. Transimpedance Amplifier Comparison

	OPA380	**TL084**	**OPA320**
Price	\$6	\$0.50	\$2.50
Input noise	5.8 nV/$\sqrt{\text{Hz}}$	18 nV/$\sqrt{\text{Hz}}$	7 nV/$\sqrt{\text{Hz}}$
Slew rate	80 V/μs	80 V/μs	10 V/μs
GBW	90 MHz	3 MHz	20 MHz

Table 10. Switching Regulator Comparison

	MP1584EN	**LMR33620**	**AP63203/05**
Price	\$3	\$3	\$1
I_Q	100 μA	25 μA	22 μA
I_{max}	3 A	2 A	2 A
Efficiency	92%	95%	95%
f_{sw}	1.5 MHz	0.4–2.1 MHz	1.1 MHz

4.1 Transimpedance Amplifier Selection

The photodiode receiver requires a transimpedance amplifier to convert its current output into a usable voltage. Table 9 compares three candidates. The TL084 was ruled out despite its low cost because its 18 nV/$\sqrt{\text{Hz}}$ input-referred noise was high enough to risk corrupting the already faint optical return signal. The OPA380 offered the best noise performance of the three, but its price premium over the OPA320 was judged not worth the marginal improvement for this application. The OPA320 was selected as the balance point between noise performance and cost.

4.2 Switching Regulator Selection

The main supply stage steps the 12 V input down at high efficiency before the linear stage cleans it up. All three candidates in Table 10 met the 12 V input requirement; the AP63203/AP63205 pair was selected for its markedly lower cost, lower quiescent current, and equivalent 95% efficiency relative to the LMR33620, while comfortably outperforming the MP1584EN on efficiency and quiescent draw.

4.3 Linear Regulator Selection

Two clean rails are required downstream of the switching stage: 3.3 V for the RF and optical front ends, and 5 V for the MCU and remaining logic. Table 11 lists six candidates. The LP2985 family was eliminated at both voltages for insufficient current handling. For the 3.3 V rail, the TLV75533PDBVR was selected over the MCP1700-3302E for its higher current capability, lower output noise, and lower cost. For the 5 V rail, the classic LM7805 offered generous input headroom, but its price premium over the L78M05CDT was judged unnecessary given that the regulator board's input is already a regulated 12 V rail rather than an unpredictable external supply; the L78M05CDT was selected instead.

4.4 Thermal Management

With every regulator dissipating some power as heat on a single densely packed board, junction temperature was checked explicitly for each part using $T_J = T_A + P_D \cdot \theta_{JA}$, with ambient T_A taken as 25°C. Table 12 shows that every regulator remains well below its rated maximum junction temperature, and the regulator board's 2 oz copper pour (Section III-F) provides further margin by spreading heat away from the densest cluster of switching components.

5. SOFTWARE DESIGN AND APPLICATION

The mobile software architecture utilizes an application built on the Flutter framework, operating entirely independent of the internet. The smartphone connects directly to the bedside lamp's localized HTTP server over a common local Wi-Fi network, ensuring biometric data never leaves the physical confines of the user's bedroom. On the embedded side, firmware is organized into five parallel sensing branches; thermal, movement, respiratory/heart rate, in-bed detection, and sound. Each of which samples its sensor, applies its own signal-processing pipeline, and writes a timestamped record to a local database table. Sample data is periodically

Table 11. Linear Regulator (LDO) Comparison

Regulator	Price	V_{in}	V_{out}	I_Q	I_{max}	Output Noise
TLV75533PDBVR	**$0.42**	**1.45–5.5 V**	**3.3 V**	**25 μA**	**500 mA**	**71.5 μV_{RMS}**
LP2985-33DBVR	$0.54	2.1–16 V	3.3 V	75 μA	150 mA	30 μV_{RMS}
MCP1700-3302E	$0.50	2.3–6 V	3.3 V	1.6 μA	250 mA	125 μV_{RMS}
LM7805	$2.00	7–35 V	5 V	6 μA	1500 mA	80 μV_{RMS}
L78M05CDT	**$0.36**	**7–35 V**	**5 V**	**4.5 μA**	**500 mA**	**80 μV_{RMS}**
LP2985-5.0	$0.60	6–16 V	5 V	75 μA	150 mA	30 μV_{RMS}

Table 12. Regulator Junction Temperature Estimates

Regulator	Type	P_D	θ_{JA}	T_J
AP63203	3.3V Switching	0.37 W	50 °C/W	43.5 °C
AP63205	5V Switching	0.17 W	50 °C/W	33.5 °C
TLV5533PDBVR	3.3V Linear	0.0165 W	250 °C/W	29.1 °C
L78M05CDT	5V Linear	0.025 W	60 °C/W	26.5 °C

bundled into a JSON payload and served to the mobile application over a lightweight HTTP/TCP server hosted directly on the ESP32-S3.

5.1 Mobile Application Technology Selection

Table 13 compares three cross-platform strategies. Fully native development (Swift/Kotlin) offered the best raw performance but was set aside given the doubled development effort of maintaining two codebases on a single-semester timeline. React Native's single codebase was attractive, but its JavaScript bridge risked introducing parsing bottlenecks against the ESP32's comparatively dense JSON telemetry arrays. Flutter was ultimately selected: its Dart codebase compiles directly to native ARM through a dedicated engine, giving consistent UI behavior and fast background parsing while roughly halving development time relative to native, a decisive factor given the team's existing familiarity with Dart.

5.2 Thermal Data Processing

Each sampling period, the MLX90640 returns a 768-pixel frame over I2C. The frame is sorted from coldest to hottest using a standard library sort, and an iterative bisection is applied: the midpoint between the minimum and maximum values is taken as a pivot, the array is split into "cold" and "hot" buckets around that pivot, and the mean of each bucket becomes the next pivot. After ten iterations this process converges on a stable estimate of ambient room temperature, discarding transient hot or cold outliers in the frame. Hotspot tracking then falls out almost for free, since the sorted array's final element is the current maximum i.e., body – temperature. A physiological sleep-onset estimate is layered on top: a baseline temperature is captured while the user is known to be awake, and the system continuously tracks the delta between that baseline and the current hotspot reading, flagging likely sleep onset once the drop exceeds a configurable 1–2°C threshold.

5.3 Movement, Respiratory, and Heart-Rate Processing

Because the MR24BSD1's onboard DSP performs its own signal decomposition internally, the MCU's role is comparatively lightweight: it issues packet requests over UART and parses the returned frames through a heavily modified version of the manufacturer's library. In practice, the manufacturer's published library proved incomplete or missing functions to gather/decode several advertised metrics, along with certain packet cases, were left unhandled in the provided source. The team worked through the raw protocol documentation to decode these packets manually and extended the library to cover the missing cases before the sensor could be trusted for testing. The resulting library exposes dedicated calls for sleep-state decoding (breath state, bed state, sleep stage, duration, and score) and for simultaneous occupancy/motion judgment, the latter tuned with empirically chosen thresholds to reduce spurious restless-movement events reported to the application.

Table 13. Mobile Application Framework Comparison

Technology	Architecture	Pros	Cons	Selection
Native	Swift (iOS) / Kotlin (Android).	Maximum performance and deep hardware access.	Two separate codebases double development time.	Overhead too high for the timeline.
React Native	JavaScript bridge to native UI components.	Single codebase; large web-developer community.	JS bridge can bottleneck on large JSON arrays.	Parsing efficiency is critical for the ESP32's dense telemetry.
Flutter	**Dart compiled to native ARM via a dedicated engine.**	**Fast execution, consistent cross-platform UI, strong background parsing.**	**Slightly larger compiled app size.**	**Selected frameworks shorten development time and matches team familiarity.**

Table 14. Audio Storage Format Comparison

	WAV	**LAME MP3**	**AAC**
CPU load	Negligible	Real-time	Very high
Storage	Massive	Low	Low
Transfer	Heavyweight	Lightweight	Efficient
Memory	Low	Moderate	High

5.4 Audio Capture and Encoding

Three audio storage strategies were compared (Table 14). Uncompressed WAV was rejected for its outsized storage footprint and heavyweight SD writes; AAC was rejected for demanding far more processing headroom and memory than the platform comfortably offers. The open-source LAME MP3 encoder was selected as the middle ground. Real-time CPU encoding and moderate memory use are both well within the ESP32-S3's available headroom, and its compressed output is both SD-friendly and simple to transfer to the mobile application. In operation, a baseline noise floor is established by averaging repeated decibel readings; live readings are then compared against that baseline, and any excursion above threshold triggers a fixed-duration recording that is streamed through the LAME encoder and written to SD as MP3 frames.

5.5 In-Bed Presence Detection Algorithm

The MCU drives the emitter LED through a transistor stage, since a GPIO pin alone cannot source sufficient current (only inputting eighth of the required power, 10 mA); the LED is modulated at 1 kHz and sampled at roughly 800 Hz. On-state and off-state readings are separately averaged to isolate the modulated return from ambient light, and a 3-second calibration window establishes a baseline intensity when the bed is known to be empty. Presence is then flagged from the percentage deviation of the live reading against that baseline rather than from absolute intensity, since this is far more robust to differences in ambient lighting between bedrooms. This threshold has itself been an active tuning target: at the midterm demo a $\geq$9% deviation was used to flag occupancy, distinguishing it from the $\sim$6% fluctuations attributable to sensor and ambient noise; by the critical design review, additional field data had led the team to lower the operating threshold to 6%, with 12% under evaluation as a less sensitive alternative should the lower threshold prove too prone to false triggers in continued testing.

6. SYSTEM TESTING AND EVALUATION

6.1 Hardware Subsystem Testing

At power-up, the firmware executes a fixed initialization sequence; SD card mount, radar configuration and sensitivity handshake, microphone initialization, HTTP server (port 80) and TCP server (port 3333) bring-up, Wi-Fi association, and an audio baseline measurement, before entering its normal sampling loop. In bench testing from a live bedroom setup, this sequence reliably brought up all four subsystems and began streaming

Table 15. Performance Against Reference Instruments

Metric	Reference	Agreement
Respiratory rate	Manual breath count	±1 BPM
Heart rate	Wrist-worn monitor	±2 BPM
Ambient temp.	Temtop air-quality monitor	∼3°F
Body (skin) temp.	Skin-contact thermometer	6°F
Audio noise floor	External SPL meter	∼2.7 dB

breath state, live heart rate, live respiratory rate, and movement events to the console within the required synchronization window (Table 2).

The optical board went through two revisions: the first prototype had a routing error on the IR receiver's supply voltage and the transimpedance amplifier stage initially had to be removed because it drove the receiver into an unreadable saturated output; the corrected board resolved both issues while preserving the three-stage emit/amplify/rank design of Section III-D. The regulator board likewise went through revision: version 1 correctly cascaded the switching and linear stages but imported an incorrect pin order for the 3.3 V linear regulator from its Ultra Librarian footprint; version 2 corrected the pin mapping but introduced several isolated ground islands, which were resolved in the final board used for testing.

The lamp housing was validated with the radar mounted behind a 2 mm-thick printed wall section to confirm through-wall sensitivity was retained, per the technology comparison in Section III-B. All boards mount to a shared inner plate via heat-fit threaded inserts and a custom-cut $\frac{1}{4}$-in threaded steel rod running from the base through the inner pillar, with the LED/photodiode pair mounted to the pillar behind a shrouded window.

6.2 Software and Application Testing

The mobile application was exercised against the live hardware over four primary views. The Dashboard reports connection status, firmware version, free storage, and averaged telemetry across all active sensors. The Sleep tab layers live and historical readings; heart rate, respiratory rate, restless-movement events, and sample counts onto time-series graphs, with an explicit in-bed/out-of-bed state indicator; because these sessions were recorded on an unattended bench rather than a sleeping subject, the reported average values (e.g., single-digit to low-double-digit bpm ranges) reflect sensor and environment calibration during bring-up rather than physiological data from an actual sleeper. The Settings tab is a developer-facing debug view exposing the target IP, HTTP/TCP ports, and poll interval used for the connection shown in Fig. 1. The Schedule & Config tab allows the end user to set an active monitoring window (demonstrated at 22:00–07:00), audio recording interval and clip duration, sensor poll interval, and the restless-movement threshold discussed in Section V-E, all of which are pushed back to the MCU as a JSON configuration update.

6.3 Performance Evaluation

Table 15 summarizes accuracy against independent reference instruments. The 24 GHz mmWave radar subsystem showed respiratory rate measurements within ±1 BPM compared to the reference method, and heart rate within ±2 BPM of a wrist-worn monitor. Thermal monitoring demonstrated stability within a 2°F margin of the reference device over a one-hour bench-stability test; in a separate evaluation against an external skin-contact thermometer, body temperature agreed within 6°F, a gap the team attributes to the well-known difference between radiometric skin-surface sensing and direct-contact measurement rather than to sensor drift. Ambient temperature and the audio noise floor both agreed with their respective reference instruments to within a few units of their own scale.

7. BUDGET

The project was allocated a $1,000 budget. As itemized in Table 16, total spend came in at approximately $672, leaving roughly a third of the original allocation unspent even after setting aside a dedicated contingency reserve.

Table 16. Project Budget by Subsystem

Subsystem	Major Components	Cost
Optical	TSAL6400 LEDs (×8), photodiodes (×5), aspheric condenser lenses (×2), misc.	$158.44
Electronics	Photodiode amp, 12 V adapter, barrel jack, buck/linear regulators, passives, protection circuitry, PCB fab.	$134.01
Embedded Sys.	Storage, MCU, radar module, microphone, MLX90640, SD interface, PCB fab.	$208.43
Contingency	Budget reserve for failures/rework.	$170.34
Total		**≈$672**

8. FUTURE WORK

With the midterm demo complete, the remaining project milestones consist of; final builds/assembly, unit testing, data gathering, and a final live demonstration. The specific milestones carried into this final stretch are:

- Finish the housing design around the now-completed subsystems, resolving the remaining shroud-fit revisions.
- Integrate the LED lamp element into the fully assembled system.
- Consolidate the application's testing menus into a single, polished, user-facing dashboard.
- Add in-application audio-clip playback.
- Conduct further long-term overnight sleep-study testing under real conditions.
- Finalize system, application, and testing data for the final live demonstration.

9. CONCLUSION

Noctisense implements a cohesive system for tracking biometric sleep data with a focus on affordability, security, and unintrusive design. It demonstrates that a high-quality, consumer-grade biometric device can operate entirely on-device without sacrificing functionality or user experience. Hardware and software testing through the critical design review stage show radar-derived vital signs, thermal readings, and audio detection all tracking within a few percent of independent reference instruments, at roughly two-thirds of the team's allocated $1,000 budget. The remaining project work is focused less on core sensing accuracy, which has already been validated subsystem by subsystem, and more on integration: finishing the housing, consolidating the application into a single user-facing dashboard, and gathering longer-duration overnight data ahead of the final live demonstration.

REFERENCES

[1] Kwon, J. H. et al., "40 years of actigraphy in sleep medicine and current state of the art algorithms," *npj Digital Medicine* **6**, 87 (2023).

[2] Grand View Research, Inc., "Sleep tracking devices market size, share & trends analysis report." https://www.grandviewresearch.com/industry-analysis/sleep-tracking-devices-market-report (2024). Accessed June 2026.

[3] Eight Sleep, Inc., "Eight sleep." https://www.eightsleep.com. Accessed June 2026.

[4] Espressif Systems, *ESP32-S3 Series Datasheet*, version 2.9 ed. (2025).

[5] Seeed Studio, "Mr24bsd1 24 ghz mmwave radar sensor for respiratory and sleep detection." https://www.seeedstudio.com/24GHz-mmWave-Radar-Sensor-Sleep-Breathing-Monitoring-Module-p-5304.html (2024). Accessed June 2026.

[6] Melexis NV, *MLX90640 Far Infrared Thermal Sensor Array Datasheet*, rev. 12 ed. (2023).